Available online at www.sciencedirect.com
SCIENCE DIRECT®
International Journal of Heat and Fluid Flow 25 (2004) 636–648
International Journal of HEAT AND FLUID FLOW
www.elsevier.com/locate/ijhff

An experimental characterization of cross-flow cooling of air via an in-line elliptical tube array

Mesbah G. Khan, Amir Fartaj, David S.-K. Ting *

Department of Mechanical, Automotive and Materials Engineering, University of Windsor, Windsor, Ont., Canada N9B 3P4

Received 2 September 2003; accepted 17 January 2004
Available online 27 February 2004

Abstract

Flows of hot air at 41.5 ± 1.5 °C across an array of elliptical tubes carrying cold water were experimentally investigated in the range of waterside and airside Reynolds numbers of $1.0 \times 10^3 < Re_w < 3.7 \times 10^3$ and $1.0 \times 10^4 < Re_a < 3.3 \times 10^4$ respectively. The waterside Reynolds number was based on the inner hydraulic diameter and that of the airside, on the major axis length of the tube. Cold water at 6.5 ± 1.0 °C entered and jig jagged through a single passage tube array, and exited at a temperature dictated by the total heat transferred. The array consisting of 18 elliptical tubes each 30 cm long, with minor to major outside axis ratio of 0.30, and equally spaced by 0.61 cm gap, was oriented at zero angle of attack in a 30 cm by 30 cm test section with the major axis parallel to the air flow. The results showed that the heat transfer rate (q) increased with the increase of both water and air flows. The pressure coefficient (C_p), across a single tube in the array was found to remain at approximately 0.16 for $Re_a > 2 \times 10^4$. Both q and Nusselt number (Nu) were found to vary in power law relationship with Re. The Nu–Re correlation obtained from the idealized test bench was found to be in the form $Nu_a = 0.26 Re_a^{0.66}$.

Keywords: Forced convection; Elliptical tube array; Cross-flow cooling

1. Introduction

Heat exchangers have been playing a vital role in energy applications for a long time. Economic and environmental issues progressively place the needs for compactness and performance improvement of such systems. In this regard, cylinders of various shapes have been studied and utilized extensively. Flow around tubes is not necessarily always normal to the tube axis, and when this is the case the cross section of a circular tube in the flow direction becomes an ellipse. An elliptic cylinder is thus a generic shape, which in special cases can represent a flat plate or circular cylinder depending on its axis ratio (AR). For example, at minor-to-major, AR of zero, infinity and 1, it represents a horizontal flat plate, vertical flat plate and circular cylinder respectively. The parameters, such as the cylinder spacing and orientations also affect the heat transfer rates. Pressure drop across the cylinder, which depends on the flow behaviors and cylinder profiles, contributes to the system performance. Other factors including flow-induced vibration and structural sustainability are also important for the system design.

An earlier but comprehensive report on cross-flow around cylinders of arbitrary cross section presented by Eckert and Livingood (1953) compared the effects of tube axis ratio on heat transfer. Their investigations were based on exact solutions of the laminar boundary layer equations. They compared their results with other analytical methods and the then available experimental results. For their investigated elliptical cylinders (axis ratios of 0.25 and 0.50), the major axis was used to define the Reynolds and Nusselt numbers. From their graphical representations, it is seen that the heat transfer coefficient is higher for elliptical cylinders than circular ones. It is also observed that the elliptical cylinder with the smaller axis ratio has higher heat transfer coefficient. Brauer (1964) demonstrated that the drag coefficient for an elliptic tube is less than that for the circular one due to its more streamlined contour. The pressure drop is

* Corresponding author. Tel.: +1-519-253-3000x2599; fax: +1-519-973-7007.
E-mail address: dting@uwindsor.ca (D.S.-K. Ting).

0142-727X/$ - see front matter © 2004 Elsevier Inc. All rights reserved.
doi:10.1016/j.ijheatfluidflow.2004.01.002

Nomenclature

a	semi-major axis length of elliptic tube [m]
A_c	cross-sectional area of the tube [m^2]; $A_c = \pi ab$
AR	axis ratio (ratio of minor-to-major axis lengths of elliptic tube); AR $= \frac{b}{a} = \sqrt{1-e^2}$
A_s	tube surface area [m^2]; $A_s = Pl_t$
b	semi-minor axis length of elliptic tube [m]
$C_1, \ldots, C_8$	correlation/curve fit coefficients
C_p	pressure coefficient; $C_p = \Delta p/0.5n\rho V_a^2$
c_p	specific heat capacity at constant pressure [kJ/kg °C]
D_h	hydraulic diameter of elliptical tube [m]; $D_h = 4A_c/P$
e	eccentricity of elliptic tube; $e = \frac{\sqrt{a^2-b^2}}{a}$
f	friction factor of elliptic tube at water side
Gr	Grashof number; $Gr = \frac{g\rho^2\beta(T_a-T_s)Z^3}{\mu^2}$; $Z = D_h$ (for waterside) and $2a_o$ (for airside)
h	average heat transfer coefficient [W/m^2 °C]
k	thermal conductivity [W/m °C]
l_t	total length of the tubes (excluding the 180° Plexiglas bends) [m]
$\dot{m}$	mass flow rate [kg/s]
n	number of tubes
Nu	average Nusselt number; $Nu_a = h_a D_{h,o}/k_a$ and $Nu_w = h_w D_{h,i}/k_w$
P	perimeter of the elliptic tube [m]
Pr	Prandtl number; $Pr = \nu/\alpha = (\mu c_p)/k$
q	heat transfer rate [kW]
R_{th}	thermal resistance [°C/W]
Re	Reynolds number; $Re_a = V_a D_{h,o}/\nu_a$ and $Re_w = V_w D_{h,i}/\nu_w$
T	temperature [°C]
$T_{f,a}$	air film temperature [°C]; $T_{f,a} = (T_{a,i} + T_{s,o})/2$
$T_{w,b}$	bulk water temperature throughout the tube array [°C]; $T_{w,b} = (T_{w,i} + T_{w,o})/2$
V	mean velocity of flowing fluid [m/s]
Z	characteristic length to be used in deducing the Grashof number [m]

Greeks

β	coefficient of thermal expansion [K^{-1}]
Δp	pressure drop across the tube array [Pa]
ε	emmissivity
μ	dynamic viscosity [kg/m s]
μ_s	dynamic viscosity taken at surface temperature of the tube array [kg/m s]
ν	kinematic viscosity [m^2/s]
σ	Stefan–Boltzmann constant [W/m^2 K^4]
ρ	density [kg/m^3]

Subscripts

a	air
b	bulk
i	inlet/entry and inner side of the tube
o	outlet/exit and outer side of the tube
s	tube surface
w	water

also less compared to circular tubes. Brauer (1964) observed enhanced heat transfer as well as relative pressure drop reduction of up to 25% when utilizing the elliptical arrangement. Schulenberg (1966) reported that for a given heat transfer duty, heat exchanger built from finned elliptical tubes requires less heat transfer surface area and consumes less power for driving fans than an exchanger built from finned circular tubes. The study of Ota et al. (1987) encompassed the flow in the neighborhood of an elliptic cylinder with an axis ratio of 0.33 in the Reynolds number range (based on major axis length) from 3.5×10^4 to 1.25×10^5, where a discontinuous variation of both the drag and lift was observed. It is evidenced from these and other investigations that at cross-flow the elliptical tube performs better than the circular configuration in terms of reduced drag coefficient, pressure drop and flow induced vibration. Rocha et al. (1997) highlighted this fact in their work for circular and elliptical tubes of different profiles. They found the elliptical configuration with an eccentricity e of 0.50 (axis ratio of 0.86) and a ratio of semi-minor axis to the length of tube row of 0.23 is the most efficient one. This is for a constant Prandtl number of 0.70 in the Reynolds number range (based on hydraulic diameter) from 0 to 1.6×10^3. Matos et al. (2001) reported a 13% relative heat transfer gain due to elliptic configuration for the same flow obstruction cross-sectional area with an eccentricity of 0.65 (axis ratio of 0.75) and tube length to minor axis ratio of 6.2 for constant Prandtl number of 0.72 and Reynolds number range from 3×10^2 to 8×10^2, where Reynolds number was based on the length of tube row.

Many investigators have also studied other parameters in connection to heat transfer such as cylinder orientation, spacing, axis ratio, and angle of attack. The effects of cylinder spacing and angle of attack on heat transfer for elliptic tubes were investigated by Nishiyama et al. (1988) in tandem arrangement. They found that the angle of attack as well as the cylinder spacing influence the local heat transfer coefficient. They concluded that the cylinder spacing and the angle of attack should be arranged as small as possible to minimize the drag and to achieve higher heat transfer rate and compactness of the system. Badr (1998) conducted a numerical study with a single elliptical cylinder and investigated the effects of Reynolds number, cylinder

axis ratio and the angle of attack on heat transfer. The Reynolds number (based on twice the focal distance) varied from 20 to 500 for a constant Prandtl number of 0.70. The axis ratio was varied between 0.40 and 0.90 for zero angle of attack and for a fixed Reynolds number of 100. In addition, the angle of attack was altered from 0° to 90° for a fixed axis ratio of 0.50 for Reynolds number between 20 and 500. Badr found the maximum Nusselt number occurred at zero angle of attack and the maximum heat transfer at small axis ratio. Harris and Goldschmidt (2002) investigated the effects of axis ratio and angle of attack on overall heat transfer in the Reynolds number range from 7.4×10^3 to 7.4×10^4. Both the Reynolds and Nusselt numbers were based on the length of the major axis. They concluded that an axis ratio of 0.30 or less must be achieved to realize any appreciable change in the heat transfer coefficient (e.g. greater than 10%) over the circular tube.

Very few studies on a single-row of elliptical tube configuration have been made. Almost all of the earlier studies dealt with heating process, where hot cylinders (mostly electrically heated) at cross-flow of cold air were examined either for constant cylinder surface temperature or for uniform heat flux. For example, Badr (1998) worked with constant surface temperature and Laetitia and Kondjoyan (2002) and Ota and Nishiyama (1984) with uniform heat flux. Only a few studies focused on the cases where tube surface temperature and heat flux may not be treated as uniform. The reverse process, cooling, in which colder water passing through the elliptical tubes cools the warmer air flowing across them, has been rarely investigated. Applications of such cooling are common in air conditioning and refrigeration systems. Many applications also use the same circulating fluid to perform both heating and cooling operations in a single heat exchanger or in an integrated system, for example, integrated automotive heating and cooling applications. So the study of cooling heat transfer of tubes at cross-flow is equally important. There exist a number of studies, which compare the transfer rates of a single tube with an array or bank of tubes. As cited by Žhukauskas and Ulinskas (1988), heat transfer for single tubes and banks of tubes are similar. However, a survey of literature and compilation works by Žhukauskas (1972) reveals that the intensity of the heat transfer of a tube in a bank or array can be significantly higher than that of a single tube, depending on the arrangement of the tubes.

In the present study the cooling process was experimentally examined. An array of elliptical tubes of axis ratio 0.30 was placed at zero degree angle of attack. Airside Reynolds number, based on the mean free stream air velocity and outer major axis length of the tube, was varied from 1.0×10^4 to 3.3×10^4, while that based on the mean water velocity inside tube and inner hydraulic diameter of the tube was altered from 1×10^3 to 3.7×10^3, to observe the effects of Reynolds number on heat transfer rate and air pressure drop across the heat exchanger.

2. Experimental details and data collection

The experiment was conducted in a closed-circuit thermal wind tunnel test facility, as shown in Fig. 1a, with a contraction ratio of 6.25. The tunnel is capable of producing an air velocity up to 30 m/s. The Plexiglas (Acrylite FF Sheet) test section is 61 cm long, 30 cm high and 30 cm wide. The elliptical tubes, drawn from 0.825 mm thick 20.60 mm inner diameter circular copper tubes (type-M, ASTM B-88) with thermal conductivity of 339 W/m °C, had outside major and minor axes lengths of 3.17 and 0.97 cm respectively, as portrayed in Fig. 2a. The tube array, shown in Figs. 1b, 2b and 3, consisting of 18 elliptical tubes each of 30.48 cm long with minor-to-major outside axis ratio of 0.30 and equally spaced by 0.61 cm gap, was oriented in the test section in such a way so that the minor and major axes were respectively perpendicular and parallel to the flow of hot air (zero angle of attack). Additional small rectangular side-passages, made of the same Plexiglas with very low thermal conductivity (0.19 W/m °C), were introduced to serve

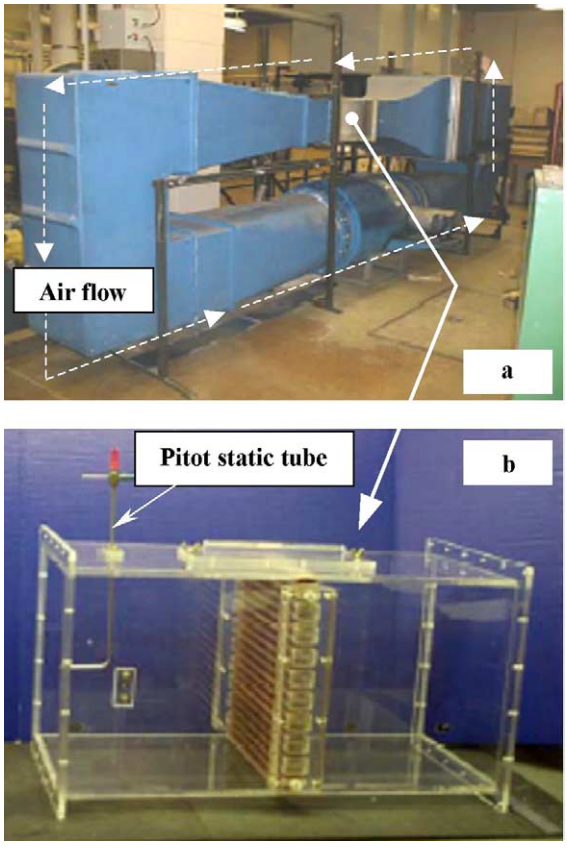

Fig. 1. (a) Closed-circuit thermal wind tunnel. (b) Test chamber with elliptical tube array.

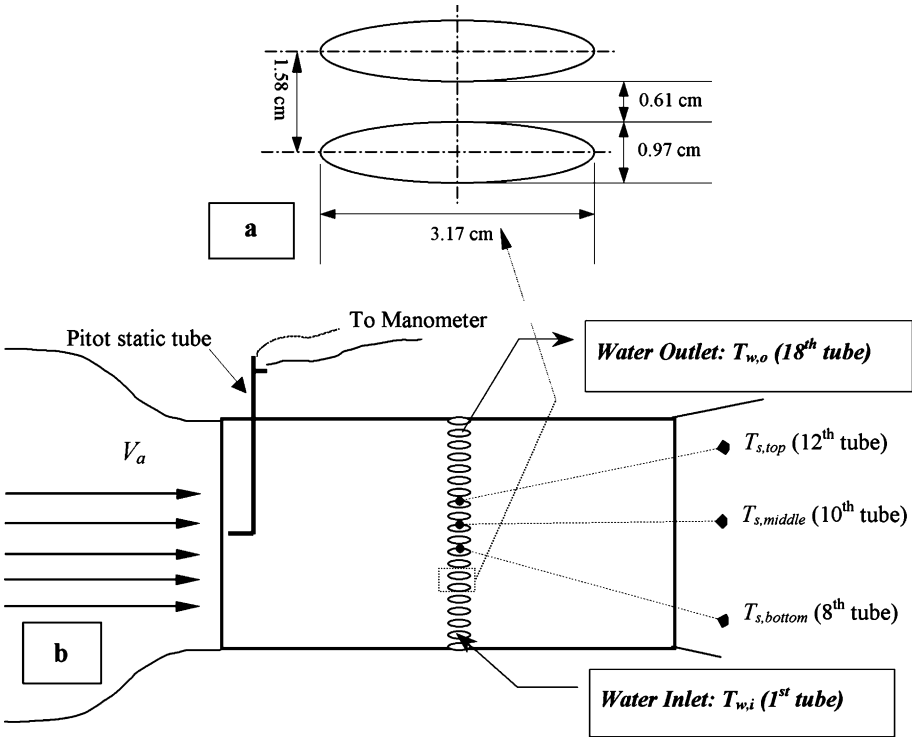

Fig. 2. Front view of the test section with measuring setup.

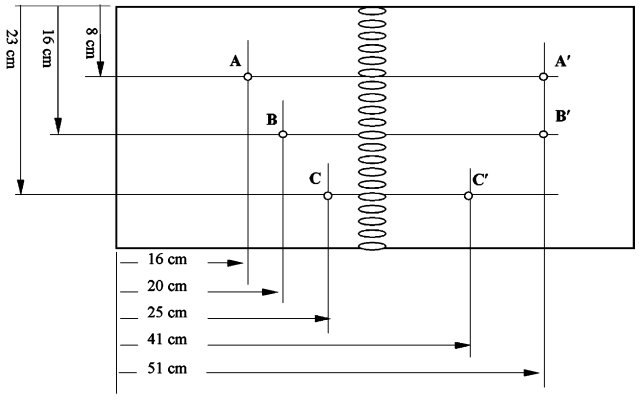

Fig. 3. Positions of the pressure tap in the test section.

the purpose of 180° bends for the tubes. The use of Plexiglas minimized the conduction heat loss through these passages. Two half dummy tubes were placed at the top and bottom of the array to minimize external strays.

A heat exchanger in the wind tunnel was the source for supplying heat to the circulating air. Air at 41.5 ± 1.5 °C entered the test section and passed over the tube array. The cold water at 6.5 ± 1.0 °C entered the tube array at the bottom (first tube) and exited at the top (18th tube) as depicted in Fig. 2b.

Four type-T thermocouples, at the water inlet and outlet of the tube array and at the air up- and downstream of the test section, were suitably placed to measure the water and air inlet and exit temperatures ($T_{w,i}$, $T_{w,o}$, $T_{a,i}$, and $T_{a,o}$); see Fig. 2b. Three additional type-T thermocouples were placed centrally and at the outside top tube surfaces of the array (at the 8th, 10th and 12th tubes counting from bottom to top excluding the two dummy tubes) to estimate the average outside tube surface temperature ($T_{s,o}$). A hand-held OMEGA HH506R digital thermometer with an uncertainty of ±(0.3 °C + 0.05% of reading) was used to record all the temperatures. The uncertainty in the temperature measurement was ±1.2 °C.

To measure the airflow pressure drop in the test section, six pressure taps were drilled as depicted in Fig. 3. The pressure drops (Δp) were measured along pressure taps A–A′, B–B′ and C–C′ using a Meriam inclined manometer with a resolution of ±0.5 mm and an accuracy of ±1 mm of Meriam gauge oil.

Sufficient times were allowed to get the air stabilized to the desired temperature and the stabilization times were observed to be roughly 30–40 min. Experimental data involved the measurements of the surface temperatures of the elliptical tubes, air inlet temperatures, water inlet and exit temperatures, and water mass flow rates corresponding to four predetermined values of mean flow air velocity in the wind tunnel. Four different cold-water mass flow rates ($\dot{m}_w$) of 0.02, 0.04, 0.06 and 0.08 kg/s were investigated. The water flow rates were measured at the beginning and end of each test using bucket-stopwatch method. The total uncertainty, including some fluctuations in the water supply line, was

approximately ±2.6% of the measured value. For each cold-water flow rate, the mean airflow velocity (V_a) was varied from 5 to 17 m/s, giving airside Reynolds numbers ranging from 1.0×10^4 to 3.3×10^4. At the air inlet ($34a_o$ upstream of the array) of the test section, a sample 5×5 grid point measurement for air velocity profile was performed in the presence of elliptical tube array heat exchanger. A nominal air velocity of $V_a \approx 10.5$ m/s was investigated during this measurement. The velocity profile was observed to be flat for the entire cross section, outside the boundary layer, with the maximum deviation of around 3% from the mean. The air velocities for subsequent experiments were measured at a single point around the center-entrance of the test section with a 2.38 mm Pitot-static tube using the same manometer as used in the pressure drop measurement. The uncertainty in air velocity measurements was roughly ±4.5% of the measured value.

3. Assumptions and data processing

In the experiment steady state flow condition was assumed. The fluid properties, for both air and water, were determined from tables given by Cengel (1998). If not mentioned otherwise, all the thermophysical properties for air were taken at film temperature, $T_{f,a}$, which ranged from 26 to 34 °C, while for water at bulk temperature, $T_{w,b}$, which varied between 6 and 15 °C.

The waterside heat gain rate was calculated by,

$$q_w = \dot{m}_w c_{p,w}(T_{w,o} - T_{w,i}), \tag{1}$$

where water inlet temperature, $T_{w,i}$ was at 6.5 ± 1.0 °C and outlet, $T_{w,o}$ changed between 9 and 22 °C from one experimental run to another depending on the heat transfer rate.

A heat balance on the test section control volume can be written as,

$$q_{total} = q_{conduction} + q_{convection} + q_{radiation}. \tag{2}$$

The conduction and radiation heat transfer between room and walls of the test section was neglected because of the very low thermal conductivity (0.19 W/m °C) of the Plexiglas and negligible temperature difference between room and outer walls of the Plexiglas. Radiation heat transfer between tube surface and warm surrounding inside test bench was also neglected. Based on measured $T_{a,i}$ and average $T_{s,o}$, the radiation heat transfer coefficients were estimated as,

$$h_{rad} = \varepsilon\sigma(T_{a,i}^2 + T_{s,o}^2)(T_{a,i} + T_{s,o}). \tag{3}$$

For commercial copper tubing with emissivity, $\varepsilon \approx 0.15$, h_{rad} was found to range from 0.91 to 0.99 W/m² °C, roughly 0.5–1.1% of the airside convective heat transfer coefficient, h_a. Thus the heat transfer between air and water was literally due solely to the convection mechanism and Eq. (2) was modified to give,

$$q_{total} \cong q_{convection} = h_a A_{s,o}(T_{a,i} - T_{s,o}), \tag{4}$$

where free-stream air temperature, $T_{a,i}$ was at 41.5 ± 1.5 °C and the mean tube outer surface temperature, $T_{s,o}$, on average changed between 11 and 25 °C from test to test.

Under steady state condition, the total heat transfer rate, q_{total}, was equal to the waterside heat gain rate, q_w. From Eq. (4) the airside average heat transfer coefficient was determined as,

$$h_a = \frac{q_w}{A_{s,o}(T_{a,i} - T_{s,o})}. \tag{5}$$

The dimensionless airside average heat transfer coefficient, i.e. the Nusselt number, was computed from,

$$Nu_a = \frac{h_a(2a_o)}{k_a}. \tag{6}$$

The average heat transfer coefficient at waterside, h_w can be estimated from,

$$h_w = \frac{q_w}{A_{s,i}(T_{s,i} - T_{w,b})}. \tag{7}$$

Since the tubes are made from copper and only 0.825 mm thick, the inner and outer surface temperatures of the tubes could be assumed to be the same,

$$T_{s,i} \cong T_{s,o}. \tag{8}$$

The dimensionless waterside average heat transfer coefficient, i.e. the Nusselt number, was computed by,

$$Nu_w = \frac{h_w D_{h,i}}{k_w}. \tag{9}$$

The issues of experimental uncertainties, as detailed in Appendix A, were addressed by consulting the ASME guideline as mentioned in the Editorial (1993) of the ASME Journal of Heat Transfer. The uncertainties in determining the q_w, Re_w, Nu_w, Re_a, Nu_a, and airflow pressure drop across tube array, Δp, were estimated and found to remain approximately within 4.5, 7, 7, 5, 6.5 and 8.8% respectively.

4. Results and discussion

The effect of natural convection on the heat transfer at airside was neglected. The maximum Grashof number, Gr_a, encountered in the experiment was approximately 1.3×10^5 giving a ratio of Gr_a/Re_a^2 of about 0.0001 ($\ll1$), which according to Incropera and DeWitt (2002), justifies the omission of natural convection.

4.1. Air-side pressure drop

The pressure drops across A–A′ and B–B′ (see Fig. 3) were observed to be roughly the same. The pressure drop across C–C′, however, was relatively higher presumably due to the near wake location of C–C′ taps. The dimensionless pressure drop, $C_p = \Delta p/0.5n\rho V_a^2$ (taken at

B–B′), is plotted against the airside Reynolds number in Fig. 4. The C_p attained a high value of 0.33 at $Re_a \approx 1.0 \times 10^4$ and sharply decreased with increasing Re_a, and then remained roughly constant at 0.16 in the range of Re_a from 2.0×10^4 to 3.3×10^4 tested. The trend showed that C_p is dependent on Re_a in the lower Re range but almost independent in the higher Re range. The total drag is a combination of friction and pressure. At low Reynolds number range the pressure coefficient, C_p, was higher and was driven significantly by friction drag, in addition to the pressure drag. With an increase in Re, the relative contribution of inertial forces increased while that of the frictional forces decreased. As the flow shifted from transition to turbulent the separation point also moved farther to the rear, reducing the size of the wake and hence the magnitude of the pressure drag.

Fig. 4 illustrates that the current C_p results are in good qualitative agreement with that of Brauer (1964) for a bundle of 20 in-line oval finned tubes with an axis ratio of 0.56. The C_p value of the in-line tube bundle presented in terms of friction factor appears to decrease asymptotically to 0.38 beyond Re_a of 3.0×10^4. The result is somewhat higher than that of the current study, which is expected because of the higher axis ratio (less streamline cylinders) and fins used by Brauer. The study by Ota et al. (1987) for a single elliptic cylinder of axis ratio 0.33 shows that at zero angle of attack the C_p remained approximately at 0.30 in the range $2.2 \times 10^4 \leqslant Re_a \leqslant 2.7 \times 10^4$. This result is also slightly higher compared to current study. This is quite reasonable, because Ota et al. used a slightly higher axis ratio than that used in the current study (0.33 versus 0.30). Overall, present result satisfactorily agreed with the trends of both Brauer and Ota et al. studies as shown in Fig. 4.

4.2. Effect of waterside Reynolds number on heat transfer

The main objective of this study was to deduce Nu_a–Re_a relationship. The Nu_w–Re_w variation is also of interest and hence, is estimated and presented here. The q as a function of Re_w was plotted in Fig. 5 and a power law relationship was obtained as,

$$q = C_1 Re_w^{C_2} \quad \text{for } 1 \times 10^3 < Re_w < 3.7 \times 10^3, \tag{10}$$

where C_1 and C_2 are the curve fit coefficients as listed in Table 2. The increase in q with respect to Re_a is clearly portrayed by the changing values of C_1 and C_2. In general, increasing Re_a increases q. The increase in q per unit increase in Re_w, $\frac{dq}{dRe_w}$, however, decreases with increasing Re_w. This is consistent with the power law effect of Re on q, that is, the effect of Re diminishes at large Re.

Average waterside heat transfer coefficient, h_w, was estimated from Eq. (7). The Nu_w corresponding to Re_w is plotted in Fig. 6 as a power law form as follows:

$$Nu_w = C_3 Re_w^{C_4} \quad \text{for } 1 \times 10^3 < Re_w < 3.7 \times 10^3, \tag{11}$$

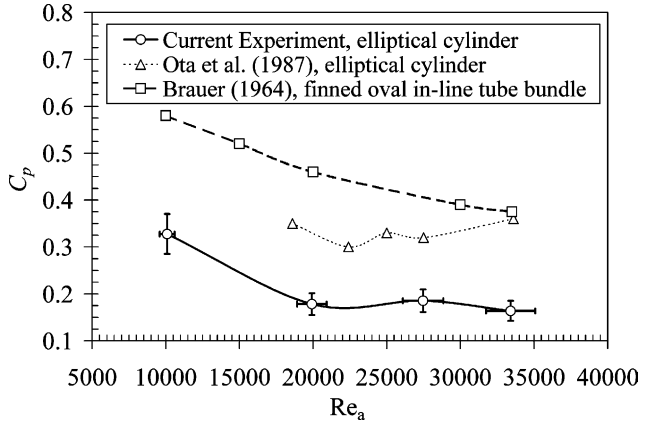

Fig. 4. Variations of C_p across test section corresponding to Re_a with error bars of typical uncertainty.

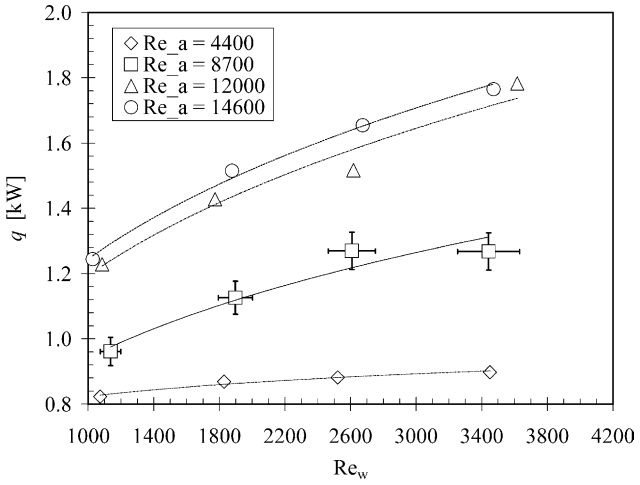

Fig. 5. Variations of q with Re_w corresponding to different air flow rates with error bars of typical uncertainty.

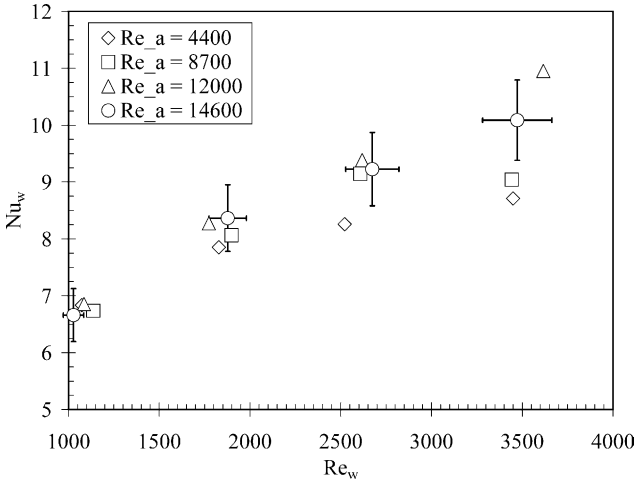

Fig. 6. Variations of Nu_w with Re_w for different airflow rates with error bars of typical uncertainty.

where C_3 and C_4 are the curve fit coefficients shown in Table 2.

From all the experimental data of Fig. 6, a relationship between the overall average Nusselt number and Reynolds number was obtained as,

$$Nu_w = 0.80 Re_w^{0.31} \quad \text{for } 1\times10^3 < Re_w < 3.7\times10^3 \text{ and } 1.0\times10^4 < Re_a < 3.3\times10^4. \tag{12}$$

This is plotted in Fig. 7. As Re_a increases, the $\frac{dq}{dRe_w}$ and $\frac{dNu_w}{dRe_w}$ also change. For low Re_a, $\frac{dq}{dRe_a}$ is large and Nu_a is relatively closer to Nu_w (e.g. $Nu_a \approx 103$ as compared to $Nu_w \approx 8$ at $Re_a \approx 1.0\times10^4$ as shown in Table 1). For the larger Re_a however, $\frac{dq}{dRe_w}$ becomes smaller and Nu_a is comparatively much larger than Nu_w (e.g. $Nu_a \approx 220$ as compared to $Nu_w \approx 9$ at $Re_a \approx 3.3\times10^4$ as shown in Table 1). Note that for $Re_a > 2.0\times10^4$, the Nu_w–Re_w relation is not affected by Re_a.

The waterside Reynolds number investigated was roughly in the range $1\times10^3 < Re_w < 3.7\times10^3$, indicating that the flow was in the laminar and transition regimes. But the tube bends, flow fluctuations from supply line and structural vibration might have caused some turbulent effects. In reality the flow probably was neither fully developed nor laminar and also not fully developed turbulent one. To check this, the experimental results were compared with available similar studies and correlations relating the Nusselt number with Reynolds number for both laminar and turbulent flow. These correlations can be very useful in determining the Nusselt number for flow inside a tube, especially when the tube surface temperature is not known or difficult to quantify. One such correlation proposed by Sieder and Tate (1936) for laminar flow inside a single straight circular tube at uniform surface temperature is

$$Nu_w = 1.86 \underbrace{\left(\frac{Re_w Pr_w}{l_t/D_{h,i}}\right)^{1/3}\left(\frac{\mu_w}{\mu_{w,s}}\right)^{0.14}}_{Y} \quad \text{for } 0.48 < Pr_w < 16{,}700, \tag{13}$$

where $\mu_{w,s}$ were taken at tube surface temperature. The use of the above equation was recommended by Whitaker (1972) for $Y \geqslant 2$. For the current experiment Y was always greater than 2. Therefore, by employing the parameters from current experiment, Eq. (13) can be reduced to $Nu_w = 0.26 Re_w^{0.43}$. This Whitaker correlation led to results, which, though slightly lower, are in satisfactory agreement with current results as shown in Fig. 7.

Another correlation for fully developed laminar flow inside smooth straight circular ducts under constant wall heat flux proposed by Shah and London (1978) and Shah and Bhatti (1987) is,

$$Nu_w = \left[1.953\left(\frac{Re_w Pr_w D_{h,i}}{l_t}\right)^{1/3}\right] \quad \text{for } \frac{Re_w Pr_w D_{h,i}}{l_t} > 100. \tag{14}$$

Introducing the conditions from current study, Eq. (14) can be re-expressed in the form of $Nu_w = 0.32 Re_w^{0.40}$. For the current study, $\frac{Re_w Pr_w D_{h,i}}{l_t}$ were less than 100. Nevertheless, results predicted using Shah correlation are in good (though somewhat lower) agreement with current values.

For the case of fully developed turbulent flow inside circular tube under constant heat flux condition, correlation suggested by Gnielinski (1976) was also compared as follows:

$$Nu_w = \frac{(f/2)(Re_w - 1000)Pr_w}{1 + 12.7(f/2)^{1/2}(Pr_w^{2/3} - 1)} \quad \text{for } 2.3\times10^3 < Re_w < 1.0\times10^4. \tag{15}$$

The pipe friction factor is evaluated from the following relation as cited by Sadik and Hongtan (2002):

$$f = (1.58 \ln Re_w - 3.28)^{-2}. \tag{16}$$

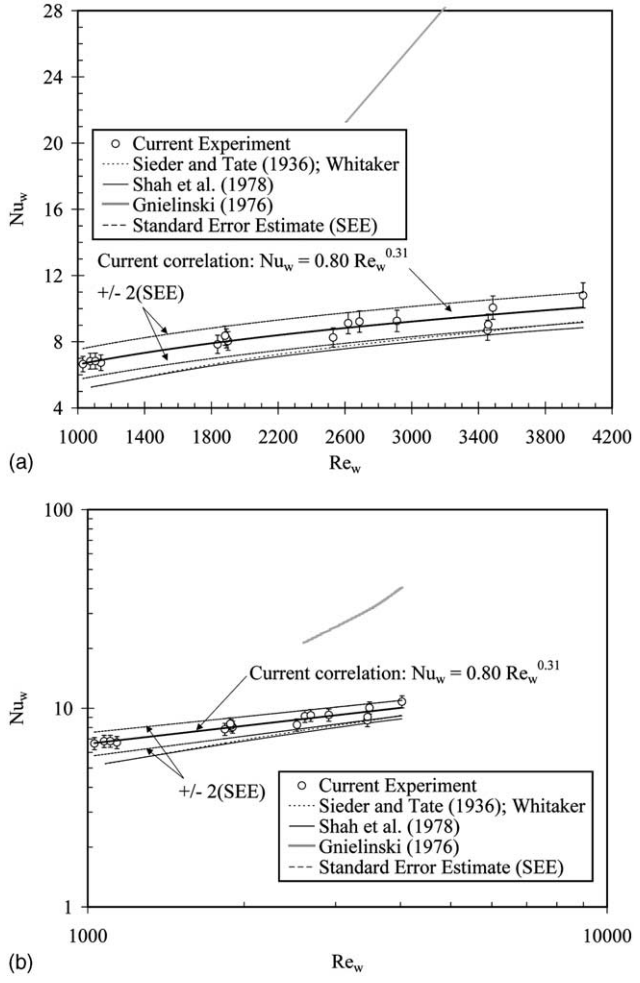

Fig. 7. (a) Variations of $\overline{Nu_w}$ with Re_w and comparisons with other correlations with error bars of typical uncertainty and standard error estimate (SEE) band; (b) log–log plot.

Table 1
Comparisons of water- and airside Nusselt numbers corresponding to different Re_w and Re_a investigated

Waterside		Airside	Airside Nusselt number, Nu_a		
Reynolds number, $Re_w \times 10^{-3}$	Nusselt number, Nu_w	Reynolds number, $Re_a \times 10^{-3}$	Current experimental values	Žhukauskas (1972); Eq. (20)	Ota and Nishiyama (1984); Eq. (21)
1.1	6.8	9.9	112	60	79
1.8	7.9	10.0	103	61	80
2.5	8.3	10.1	100	61	80
3.5	8.7	10.2	99	61	80
1.1	6.7	19.9	167	91	115
1.9	8.1	19.9	159	91	115
2.6	9.1	19.9	166	91	115
3.4	9.0	19.9	158	91	115
1.1	6.9	27.3	216	110	137
1.8	8.3	27.4	205	110	137
2.6	9.4	27.5	198	111	137
3.6	11.0	27.7	225	111	138
1.0	6.7	33.1	225	124	152
1.9	8.4	33.4	215	124	152
2.7	9.2	33.5	219	125	153
3.5	10.0	33.6	224	125	153

Table 2
Curve fit coefficients for waterside calculations

Curve fit coefficients for Eq. (10)			Curve fit coefficients for Eq. (11)		
$Re_a \times 10^{-3}$	C_1 [kW]	C_2	$Re_a \times 10^{-3}$	C_3	C_4
10.1	0.49	0.07	10.1	1.63	0.21
19.9	0.15	0.27	19.9	0.92	0.29
27.5	0.16	0.29	27.5	0.48	0.38
33.4	0.17	0.29	33.4	0.64	0.34

The effect of thermal boundary conditions can be neglected in turbulent forced convection, as mentioned by Sadik and Hongtan (2002), and correlation (15) can be used for both constant wall heat flux and constant wall surface temperature. Fig. 7 shows that Gnielinski's correlation for turbulent flow, $Nu_w = 0.0006Re_w^{1.34}$, highly over-predicted the waterside Nusselt number, compared to current experimental results. This is expected as the turbulence lowers the Nu_a resistance and $\frac{dNu}{dRe}$ is relatively much larger for turbulent flow.

The current experimental results agree reasonably well, both qualitatively and quantitatively, with correlations proposed by Sieder and Tate (1936), Shah and London (1978), and Shah and Bhatti (1987). As expected, the present Nu_w values are somewhat higher, due presumably to the flow disturbance caused by the bends as mentioned before. It is obvious that the Reynolds number is a key factor affecting the heat transfer.

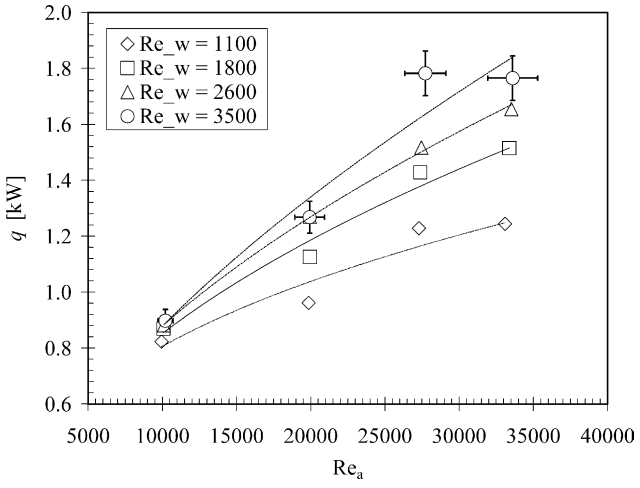

Fig. 8. Variations of q with Re_a corresponding to water mass flow rates with error bars of typical uncertainty.

4.3. Effect of airside Reynolds number on heat transfer

The heat transfer rate as a function of airside Reynolds number was plotted in Fig. 8 and a power law relationship between them was obtained as,

$$q = C_5 Re_a^{C_6} \quad \text{for } 1.0 \times 10^4 < Re_a < 3.3 \times 10^4, \tag{17}$$

where C_5 and C_6 are the curve fit coefficients listed in Table 3. The expected power law correlation indicates a decreasing Re_a enhancement $\left(\frac{dq}{dRe_a}\right)$ effect with increasing Re_a. In other words, increasing Re_a at low Re_a agitates the boundary layer and hence increases q, further increase in Re_a leads to progressively lesser boundary layer

Table 3
Curve fit coefficients for Airside calculations

Curve fit coefficients for Eq. (17)			Curve fit coefficients for Eq. (18)		
$Re_w \times 10^{-3}$	C_5 [kW]	C_6	$Re_w \times 10^{-3}$	C_7	C_8
1.1	0.028	0.37	1.1	0.42	0.61
1.8	0.010	0.48	1.8	0.29	0.64
2.6	0.007	0.53	2.6	0.23	0.66
3.5	0.003	0.61	3.5	0.11	0.74

alteration. The increase in q with respect to Re_w can also be seen from the change of C_5 and C_6 values in Fig. 8.

Fig. 9 shows the variations of average Nusselt number with Reynolds number. Nusselt number increased with the increase of Reynolds number in the power law fashion,

$$Nu_a = C_7 Re_a^{C_8} \quad \text{for } 1.0 \times 10^4 < Re_a < 3.3 \times 10^4 \text{ and } 1 \times 10^3 < Re_w < 3.7 \times 10^3, \tag{18}$$

where C_7 and C_8 are the curve fit coefficients given in Table 3. It was also observed that for a given Re_a, the values of Nu_a for a given Re_a for all the water mass flow rates were roughly the same. While the q–Re_a relation is affected significantly by Re_w, the corresponding Nu–Re_a is not expected to be so, as long as the thermal resistance of air is much larger than that of water e.g. $R_{th,a} \gg R_{th,w}$ (which is the case here).

With the negligible influence of Re_w, we can express an overall average Nu–Re_a relation as,

$$Nu_a = 0.26 Re_a^{0.66} \quad \text{for } 1.0 \times 10^4 Re_a < 3.3 \times 10^4 \text{ and } 1 \times 10^3 < Re_w < 3.7 \times 10^3. \tag{19}$$

This experimental correlation is compared with those of others in Fig. 10. The generalized correlation proposed by Žhukauskas (1972) and Žhukauskas and Žiugžda (1985), as referenced in Sadik et al. (1987)

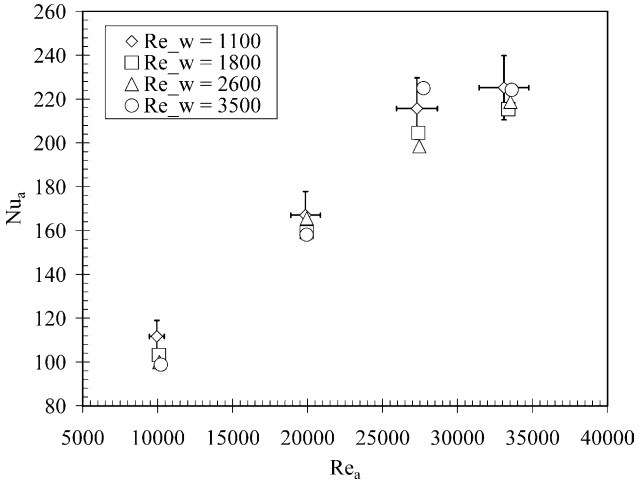

Fig. 9. Variations of Nu_a with Re_a at different water mass flow rates with error bars of typical uncertainty.

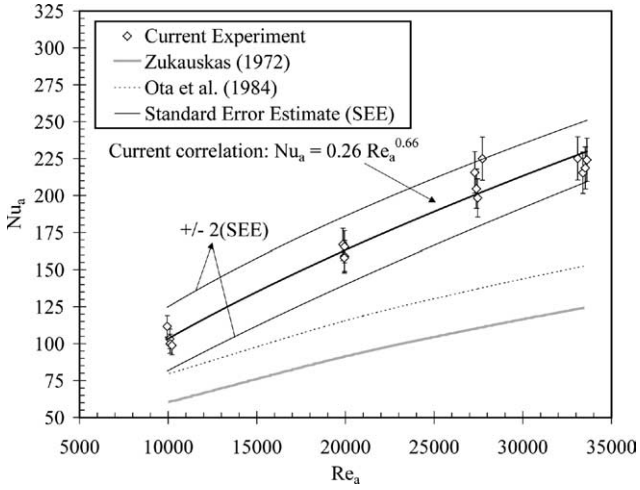

Fig. 10. Variations of $\overline{Nu_a}$ with Re_a and comparison with different correlations with error bars of typical uncertainty and standard error estimate (SEE) band.

$$\overline{Nu_a} = 0.27 Re_a^{0.60} Pr_a^{0.37} \left(\frac{Pr_a}{Pr_s}\right)^{0.20} \quad \text{for } 1 \times 10^3 \leqslant Re_a \leqslant 2 \times 10^5, \tag{20}$$

where Re_a was based on outer major axis of the cylinder, represents the average Nusselt number for forced convection from an elliptical cylinder at cross-flow of air under constant surface temperature and uniform heat flux conditions. If we substitute for $Pr_a = 0.71$, Žukauskas correlation gives $Nu_a = 0.24 Re_a^{0.60}$, which is in close qualitative agreement with the present study, nevertheless Žukauskas correlation predicts lower heat transfer (Nu_a), roughly 40% lower, for a given Re_a.

Another correlation for a single elliptic cylinder of axis ratio 0.33 at zero angle of attack under uniform heat flux (electrically heated) proposed by Ota and Nishiyama (1984) is,

$$Nu_a = 0.55 Re_a^{0.54} \quad \text{for } 8 \times 10^3 \leqslant Re_a \leqslant 7.9 \times 10^4, \tag{21}$$

where Re_a was based on the major axis of the tube. This expression leads to Nu–Re_a results, which also predicts lower Nu_a than current study by 29%. It is worth noting that higher Re_a range was considered by Ota and Nishiyama. Note that the correlations in Eqs. (20) and (21) were established for single elliptic cylinder, whereas a single array of elliptical tubes with axis ratio of 0.30 was

considered in the current study. According to Žhukauskas (1972) as mentioned in page 7, this array is expected to give larger Nu_a. All these might have caused some quantitative variations in result. In spite of these discrepancies in the experiments from study to study, the results from the current study have very good qualitative agreement with those of Žukauskas and Ota and Nishiyama. The reason for the scatter in the literature is due to the large spectrum of different conditions reported; e.g. angle of attack, tube bundle arrangement, elliptic axis ratio, internal and external flow regimes, characteristic length used to reduce data (minor axis, major axis or hydraulic diameter), boundary condition (uniform wall temperature or uniform heat flux), etc.

5. Concluding remarks

Forced convection cross-flow heat transfer of hot air over an array of cold water carrying elliptic tubes has been studied experimentally for airside and waterside Reynolds number in the range of $1.0 \times 10^4 < Re_a < 3.3 \times 10^4$ and $1 \times 10^3 < Re_w < 3.7 \times 10^3$ respectively. The mean flow velocities of air and water and tube major axis for airside and inner hydraulic diameter for waterside were used to define Re. The inlet temperatures of hot air and cold water were at 41.5 ± 1.5 and 6.5 ± 1.0 °C respectively. The non-dimensional pressure drop across the array (divided by the number of tubes) remained at around 0.16 for $2.0 \times 10^4 \leqslant Re_a \leqslant 3.3 \times 10^4$. The Nusselt number and hence, the heat transfer rate, increased with increasing Reynolds number in a power law fashion over the conditions considered. The airside Nusselt number–Reynolds number correlation was found to be $Nu_a = 0.26 Re_a^{0.66}$, indicating that the increment in Nu_a per unit increase in Re_a decreases with increasing Re_a. The result was compared with similar available studies and correlations, where very good qualitative agreement was found. Quantitatively the current result predicted higher heat transfer rate, which is expected because the result reported here is based on a very specific set of conditions tested (a relatively lower axis ratio and an array of tubes).

Acknowledgements

This work was supported by NSERC, the university of Windsor and ASHRAE. The lead author is most grateful to ASHRAE for its Grant-In-Aid scholarship.

Appendix A. Uncertainty analysis

The experimental uncertainity issues were dealt by following the ASME Journal of Heat Transfer Editorial (1993) and consulting some other notable works on experimental uncertainty such as Moffat (1985), Abernethy et al. (1985), Coleman and Steele (1989), etc. A few sample calculations are presented here.

For the independent parameters (like temperature, dimensions, etc.) the various bias (B) and precision errors (P) were found by using the root sum square (RSS) method,

$$B = \sqrt{B_1^2 + B_2^2 + \cdots + B_k^2} \tag{A.1}$$

and

$$P = \sqrt{P_1^2 + P_2^2 + \cdots + P_k^2}. \tag{A.2}$$

To combine the elemental errors to get their 95% confidence uncertainty (U), the following relation was used:

$$U = \sqrt{B^2 + P^2}. \tag{A.3}$$

For the dependent parameters (like q, Re, Nu, V, etc.), which are functions of other measured independent parameters, the uncertainty of the independent variable propagates into them according to their functional relationship. For example, in case of Reynolds number (Re),

$$Re_a = \frac{\rho V_a (2a_o)}{\mu_a} = \frac{V_a (2a_o)}{\nu_a}. \tag{A.4}$$

The uncertainties from velocity, tube major axis and kinematic viscosity propagate into Re, which can be estimated in terms of absolute or relative values (%) as follows:

absolute :

$$U_{Re_a} = \sqrt{\left(\frac{\partial Re_a}{\partial V_a} U_{V_a}\right)^2 + \left(\frac{\partial Re_a}{\partial (2a_o)} U_{(2a_o)}\right)^2 + \left(\frac{\partial Re_a}{\partial \nu_a} U_{\nu_a}\right)^2} \tag{A.5}$$

or

relative :

$$\left(\frac{U_{Re_a}}{Re_a}\right) = \sqrt{\left(\frac{U_{V_a}}{V_a}\right)^2 + \left(\frac{U_{(2a_o)}}{2a_o}\right)^2 + \left(\frac{U_{\nu_a}}{\nu_a}\right)^2}. \tag{A.6}$$

Eqs. (A.5) and (A.6) need the uncertainty components of U_{V_a}, $U_{(2a_o)}$ and $U\nu_a$, which are determined a priori.

To find out the zeroth order and also the first order uncertainty, the instruments' resolution and accuracy were taken to be the bias errors and from the known and judged sources of information, other associated errors (both bias and precision) are quantified.

A.1. Uncertainty in tube dimension measurements (U_{2a_o})

All the dimensions of the elliptical tube were measured for 12–25 populations using a digital caliper. The caliper has an accuracy of ±0.0000254 m and a resolution of 0.0000127 m which gave a fixed zeroth order bias error of $B_{\text{caliper}} = 2.84 \times 10^{-5}$ m. From the standard deviation of the mean and using student-t distribution at 95% confidence interval, the precision limits ($P_{\text{dimension}}$) for all the dimensional parameters were estimated and their uncertainties were calculated as,

$$U_{\text{dimension}} = \sqrt{(B_{\text{caliper}})^2 + (P_{\text{dimension}})^2}. \tag{A.7}$$

The dependent parameters like area, perimeter, hydraulic diameter, etc. were found from their functional relationship following the procedure of Eqs. (A.5) and (A.6).

A.2. Uncertainty in thermo-physical property evaluation for both air and water ($U_{property}$)

Even if there is any precision error, the uncertainty for physical property is normally taken as the bias error. According to the Editorial of ASME Journal of Heat Transfer (1993) and Coleman and Steele (1989), the uncertainty for respective thermo-physical property may be 0.25–0.5 times the absolute value or even higher. In current study, several times the temperatures were measured to give different populations of air film and water bulk temperatures, on which the property evaluation was based. The uncertainty for these properties were reasonably estimated as follows:

$$U_{\text{property}} = \tfrac{1}{2}|(\text{Property}_{@T_f,\text{a,max}} - \text{Property}_{@T_f,\text{a,min}})| \quad \text{for air} \tag{A.8}$$

and

$$U_{\text{property}} = \tfrac{1}{2}|(\text{Property}_{@T_w,\text{b,max}} - \text{Property}_{@T_w,b,\text{min}})| \quad \text{for water.} \tag{A.9}$$

A.3. Uncertainty in temperature measurements (U_T)

The mentioned thermometer has a resolution of 0.05 °C and accuracy of ±(0.05% of reading + 0.3 °C). According to Eq. (A.1), zeroth order bias is then $B_{\text{meter},0} = \pm 0.3052$ °C. The zeroth order precision error was considered to be due to the unsteadiness in reading (±0.2 °C) and error associated with readability (usually 0.5 times the least scale division of the thermometer). These were calculated to be $P_{\text{meter},0} = \pm 0.21$ °C. Bias errors in the thermocouple probe include the resolution (±0.025 °C), accuracy (±1.0 °C) and probe-to-probe variation of ±0.4 °C (because 11 thermocouples were used to measure various temperatures). The radiation to and from the probe was neglected. The temporal and spacial variations for the probes were taken to be ±0.2 and ±0.1 °C, which fall within the precision error. The zeroth order bias and precision error for thermocouple is estimated to be $B_{\text{probe},0} = \pm 1.07$ °C and $P_{\text{probe},0} = \pm 0.22$ °C. The zeroth order bias limit for the thermometer and thermocouple probe together is $B_{T,0} = \pm 1.12$ °C. This is also called the design stage uncertainty.

A.4. Uncertainty in air velocity measurements (U_{V_a})

The air velocity at test section inlet and the pressure drop across the tube array both were measured in terms of pressure difference (mm) using a Meriam inclined manometer. With its resolution and accuracy of 0.5 mm and ±1 mm respectively, the zeroth order bias was estimated to be $B_{\text{mano}} = 0.001118$ m. Introducing a readability error of ±0.5 mm (1/2 times the least scale digit) and a factor for unsteadiness in reading (±2 mm), the precision error was calculated to be $P_{\text{mano}} = 0.0022361$ m. The Pitot-static tube has to be right-aligned, but practically it may have some error. To compensate this, an installation bias error was considered to be ±1% of the measured Δp, which in current experimental situation could be 0.001 m. Thus the first order uncertainty contribution of manometer and Pitot static tube system to be $U_{l_{\text{mano}}} = U_{\Delta p,1} = 0.0032$ m. Thus the uncertainty for pressure difference was deduced as,

absolute :

$$U_{\Delta p} = \sqrt{\left(\frac{\partial \Delta p}{\partial \gamma_{H_2O}} U_{\gamma_{H_2O}}\right)^2 + \left(\frac{\partial \Delta p}{\partial l_{\text{mano}}} U_{l_{\text{mano}}}\right)^2} \tag{A.10}$$

or

relative :

$$\left(\frac{U_{\Delta p}}{\Delta p}\right) = \sqrt{\left(\frac{U_{\gamma_{H_2O}}}{\gamma_{H_2O}}\right)^2 + \left(\frac{U_{l_{\text{mano}}}}{l_{\text{mano}}}\right)^2}. \tag{A.11}$$

The air velocity is given by,

$$V_a = \sqrt{\frac{2\Delta p}{\rho_a}}. \tag{A.12}$$

From this relation, the uncertainty in air velocity was deduced as,

$$\left(\frac{U_{V_a}}{V_a}\right) = \frac{1}{2}\sqrt{\left(\frac{U_{\Delta p}}{\Delta p}\right)^2 + \left(\frac{U_{\rho_a}}{\rho_a}\right)^2}. \tag{A.13}$$

A.5. Sample calculation of uncertainty for Δp, V_a and Re_a

As a sample case, at $V_a \approx 10$ m/s, the relative uncertainty of pressure difference was found (using Eqs. (A.8)

and (A.11)) to be $U_{\Delta p}/\Delta p = 0.088155$ (8.82%). From Eqs. (A.11) and (A.13), the relative uncertainty for air velocity was found to be $U_{V_a}/V_a = 0.04457$ (4.46%). The uncertainty in airside Reynolds number can now be found using Eqs. (A.6) and (A.13) as follows:

$$\left(\frac{U_{Re_a}}{Re_a}\right) = \sqrt{\left(\frac{U_{V_a}}{V_a}\right)^2 + \left(\frac{U_{(2a_o)}}{2a_o}\right)^2 + \left(\frac{U_{v_a}}{v_a}\right)^2} = \sqrt{(0.04457)^2 + \left(\frac{7.035\times10^{-5}}{0.0317}\right)^2 + \left(\frac{4.035\times10^{-7}}{1.597\times10^{-5}}\right)^2} = 0.05128 = 5.13\%.$$

A.6. Uncertainty in water mass flow measurements ($U_{m'}$)

The stopwatch has accuracy ±0.5 s, resolution 0.25 s, and digital error (1/2 times the least digit) 0.05 s which was treated as bias errors. For precision, errors associated with readability (1/2 times the least digit = 0.05 s) and stopwatch handling error of ±2 s were accounted. This gave zeroth order bias of $B_t = \pm 0.561$ s, and zeroth order precision of $P_t = \pm 2.001$ s leading to zeroth order uncertainty of $U_t = \pm 2.078$ s. Water balance has accuracy of ±0.046 kg and resolution of 0.023 kg. This gives zeroth order bias for balance as $B_{mw} = \pm 0.05143$ kg. Precision errors considered were water fluctuation of ±0.046 kg, readability error ±0.045 kg and bucket handling error of ±0.092 kg giving an uncertainty due to balance and bucket of $U_{mw} = \pm 0.1239$ kg. These U_t and U_{mw} propagated into the mass flow rate according to $\dot{m}_w = m_w/t$ relation.

Estimation of uncertainties for other parameters not discussed here follow the same procedure.

A.7. Standard error estimate (SEE)

The error band in the correlations developed both for airside and waterside can be validated for correctness by using the standard error estimate as mentioned by Coleman and Steele (1989). First the linear correlation coefficients are calculated by the least square method and then they are used in the calculation of SEE by applying to developed power law relationship as follows:

$$\mathrm{SEE} = \sqrt{\frac{\sum_{i=1}^{N}[Nu_i - (n\,Re_i + C)]^{1/2}}{N-2}}. \qquad (A.14)$$

From the developed correlation in the current study, the linear coefficients are $n = 0.0012$ and $C = 5.68$ for waterside and $n = 0.0053$ and $C = 54.904$ for airside. In the current study SEEs are found to be 0.4558 (4–7%) for waterside and 10.98 (5–11%) for airside correlations. Considering no bias contribution in this analysis, the ±2(SEE) bands were plotted around the linear regression line in Figs. 7 and 10. This showed that the error bars fall within the SEE band plotted, which hinted that the developed correlations and curve fits were reasonable.

References

Abernethy, R.B., Benedict, R.P., Dowdell, R.B., 1985. ASME measurement uncertainty. J. Fluids Eng., Trans. ASME 107, 161–164.

Badr, H.M., 1998. Forced convection from a straight elliptical tube. Heat Mass Transfer 34, 229–236.

Brauer, H., 1964. Compact heat exchangers. Chem. Process Eng., 451–460.

Cengel, Y.A., 1998. Heat Transfer A Practical Approach. McGraw-Hill, New Jersey.

Coleman, H.W., Steele, W.G., 1989. Experimentation and uncertainty analysis for engineers. John Wiley and Sons, New York.

Eckert, E.R., Livingood, J.N.B., 1953. Method for calculation of laminar heat transfer in air flow around cylinders of arbitrary cross section. NASA-NACA Report 1118, pp. 223–251.

Editorial, 1993. Journal of Heat Transfer policy on reporting uncertainties in experimental measurements and results. J. Heat Transfer, Trans. ASME 115, 5–6.

Gnielinski, V., 1976. New equations for heat and mass transfer in turbulent pipe and channel flow. Int. Chem. Eng. 16 (2), 359–368.

Harris, D.K., Goldschmidt, V.W., 2002. Measurements of the overall heat transfer from combustion gases confined within elliptical tube heat exchangers. Exp. Therm Fluid Sci. 26, 33–37.

Incropera, F.P., DeWitt, D.P., 2002. Fundamentals of Heat and Mass Transfer, fifth ed. John Wiley and Sons.

Laetitia, G., Kondjoyan, A., 2002. Complete map out of the heat transfer coefficient at the surface of two circular cylinders H/D = 3.0 and 0.30 subjected to a cross-flow of air. Int. J. Heat Mass Transfer 45, 2597–2609.

Matos, R.S., Vargas, J.V.C., Laursen, T.A., Saboya, F.E.M., 2001. Optimization study and heat transfer comparison of staggered circular and elliptic tubes in forced convection. Int. J. Heat Mass Transfer 44, 3953–3961.

Moffat, R.J., 1985. Using uncertainty analysis in the planning of an experiment. J. Fluids Eng., Trans. ASME 107, 173–178.

Nishiyama, H., Ota, T., Matsuno, T., 1988. Heat transfer and flow around elliptic cylinders in tandem arrangement. JSME Int. J., Ser. II 31 (3), 410–419.

Ota, T., Nishiyama, H., 1984. Heat transfer and flow around an elliptic cylinder. Int. J. Heat Mass Transfer 27 (10), 1771–1779.

Ota, T., Nishiyama, H., Taoka, Y., 1987. Flow around an elliptic cylinder in the critical Reynolds number regime. J. Fluids Eng., Trans. ASME 109, 149–155.

Rocha, L.A.O., Saboya, F.E.M., Vargas, J.V.C., 1997. A comparative study of elliptical and circular sections in one- and two-row tubes and plate fin heat exchangers. Int. J. Heat Fluid Flow 18 (2), 247–252.

Sadik, K., Hongtan, L., 2002. Heat Exchangers: Selection, Rating, and Thermal Design. CRC Press LLC, Florida.

Sadik, K., Shah, R.K., Aung, W., 1987. Handbook of Single-Phase Convective Heat Transfer. John Wiley and Sons, New York.

Schulenberg, F.J., 1966. Finned elliptical tubes and their application in air-cooled heat exchangers. Trans. ASME, 179–190.

Shah, R.K., Bhatti, M.S., 1987. Laminar convective heat transfer in ducts. In: Kakac, S., Shah, R.K, Aung, W. (Eds.), Handbook of Single-Phase Convective Heat Transfer. John Wiley and Sons, New York (Chapter 3).

Shah, R.K., London, A.L., 1978. Laminar Forced Convection in Ducts. Academic Press, NY.

Sieder, E.N., Tate, G.E., 1936. Heat transfer and pressure drop of liquids in tubes. Ind. Eng. Chem. 28, 1429–1436.

Whitaker, S., 1972. Forced convection heat transfer correlations for flow in pipes, past flat plates, single cylinders, single spheres, and flow in packed beds and tubes. AIChE J. 18, 361–371.

Žhukauskas, A., 1972. Heat transfer from tubes in cross flow. In: Advances in Heat Transfer, vol. 8. Academic Press, New York, pp. 93–160.

Žhukauskas, A., Ulinskas, R., 1988. Heat Transfer in Tube Banks in Cross Flow. Hemisphere Publishing Corporation, Washington.

Žhukauskas, A., Žiugžda, R., 1985. Heat Transfer of a Cylinder in Cross Flow. Hemisphere Publishing Corporation, Washington.